CrossMark

ORIGINAL PAPER

# Preparation and dielectric properties of PVP-based polymer electrolyte films for solid-state battery application

S. K. Shahenoor Basha[1] · G. Sunita Sundari[1] ·
K. Vijay Kumar[2] · M. C. Rao[3]

**Abstract** Solid polymer electrolyte has been prepared with the combination of PVP (poly vinyl pyrrolidone) and magnesium sulfate heptahydrate ($MgSO_4 \cdot 7H_2O$) by solution cast technique and subsequently characterized for possible polymer battery application. Structural studies were carried out by XRD technique. DSC analysis revealed that the micro-porous polymer membrane is thermally stable up to 300 °C. The surface morphology of the films was analyzed by SEM. Electrical conductivity was performed using AC impedance analyzing technique in the frequency range from 4 kHz to 5 MHz. Complex impedance spectroscopy revealed that the enhancement in electrical conductivity by salt doping and the conductivity maximum was obtained for 15 wt% of $MgSO_4 \cdot 7H_2O$ salt concentration. Optical absorption studies were carried out on to the prepared films in the wavelength range 200–600 nm. Solid-state polymer battery has been fabricated with the configuration of $Mg^+/(PVP + MgSO_4 \cdot 7H_2O)/(I_2 + C + electrolyte)$ and discharge characteristics were studied for a constant load of 100 kΩ. The cell parameters like open-circuit voltage, short circuit current, energy density and power density were calculated.

**Keywords** PVP · XRD · DSC · SEM · Optical · Dielectric properties · Discharge characteristics

✉ M. C. Rao
raomc72@gmail.com

1 Solid State Ionics Laboratory, Department of Physics, K. L. University, Guntur 522502, India

2 Department of Physics, Dayananda Sagar Academy of Technology and Management, Udayapura, Bangalore 560 082, India

3 Department of Physics, Andhra Loyola College, Vijayawada 520008, India

🖄 Springer

## Introduction

The development of inorganic/polymer materials has received significant interest due to the wide range of potential applications in optoelectronic devices and electromagnetic interference shielding. Solid polymer electrolytes were made an attractive attention due to their wide range and various advantageous properties. Physically polymer electrolytes behave like solids but internal structure, ionic conductivity behavior closely resembles liquid state, i.e., free movement of ions in an electrolyte [1, 2]. The combination of inorganic salt and the polymer enhances the ionic conductivity and is related to the glass transition temperature ($T_g$) as well as inter-linking of the polymer chain, having excellent properties like high ionic conductivity, good mechanical strength, high thermal, electrical properties and having ability to form thin films easily. Flexibility, light weight, elasticity and high energy density make them suitable candidates for many electrochemical devices including solid-sate batteries, super capacitors, fuel cells, sensors, display devices, dye sensitized solar cells etc. [3–11]. Some fundamental problems and questions are still unsolved. Among them, low ionic conductivity, low cation transference number at ambient temperature and the formation of resistive layers on the electrode–electrolyte interface are crucial. To overcome these problems, various modifications of polymer salt complexes have been explored but the successes are limited [12].

Polymer electrolyte mechanism is explained by free surface (polymer air interface) and the polymer substrate interface in perturbing the $T_g$ response [13, 14]. With this model, in a sufficiently thin layer adjacent to a free surface, $T_g$ decreases due to reduced requirements for cooperative segmental mobility, thereby enhancing mobility and decreasing $T_g$ in the layer close to the substrate; $T_g$ increases if the polymer has attractive interactions with the substrate. The improvement in the mechanical properties has been explained on the premise that the filler particles act as supporting matrix for the conducting polymer electrolytes so as to retain an overall solid structure, even at high temperatures. All these physical properties, once optimized, would make them suitable candidates for solid-state ionic device applications [15, 16]. Abdelrazek has reported the physical properties of $Mg^{2+}$ filled PMMA films for optical applications [17]. Pandey et al. have prepared magnesium ion conducting gel polymer electrolytes dispersed with fumed silica for rechargeable magnesium battery application [18]. Chu and Jaipal Reddy studied the PEO-Mg polymer electrolyte system [19].

Poly vinyl pyrrolidone polymer has received special attention among the other conjugated polymers due to its good environmental stability. Poly vinyl pyrrolidone is also known as polyvidone or povidone. The structure of PVP is an arrangement of monomer N vinylepyrolidone. PVP was first synthesized by Prof. Walter Reppe and a patent was filed in 1939 for one of the most interesting derivatives of acetylene chemistry [20]. Due to the potential nature, PVP is used for energy stored devices with high capacity mainly dependent on electrical and optical properties. Chemically PVP has been bound to be inert, nontoxic and it displays a strong tendency for complex formation with a wide variety of smaller molecules [21]. PVP polymer is easily soluble in water and other polar solvents due to its molecular

structure. It has excellent properties like absorbing the moisture (wetting) and readily forming films. This makes it good as a coating or an additive to coatings [22, 23].

The local modification of the chemical structure induces drastic changes in electronic properties. SPEs are formed by adsorbing a certain amount of liquid electrolyte in a polymer framework. The polymer is the bone to maintain the physical strength and shape of the electrolyte [24–26]. The search for $Mg^{2+}$ ion containing polymer electrolytes can be interesting not only for understanding the multivalent cationic conductivity mechanism in the polymer, but also due to their lower cost and ease of handling and fabrication as thin film membranes and satisfy several requirements, including high ionic conductivity, good mechanical strength and excellent electrochemical stability. Li metal, but $Li^+$ salts suffer from several operational limitations, viz. difficulty in handling in open ambience due to highly reactive materials, high cost, etc. Indeed, materials showing $Mg^{2+}$ conductivity are quite interesting due to the advantages: (1) the ionic radii of $Li^+$ and $Mg^{2+}$ are 68 and 65 pm, respectively, i.e., comparable in magnitude. Hence, easy replacement of $Li^+$ ions by $Mg^{2+}$ ions in insertion compounds is possible. Magnesium has been successfully employed as anode in the primary and reserve batteries. (2) Magnesium metal is more stable than the lithium. It can be handled safely in oxygen and humid atmospheres unlike lithium which requires high purity argon or helium atmosphere. Therefore, safety problems associated with magnesium metal are minimal. Thus, solid-state rechargeable batteries based on $Mg/Mg^{2+}$ ion salt SPEs look very attractive as they are expected to give battery performance capabilities close to those of $Li/Li^+$ ion SPE batteries due to the fact that $Mg^{2+}$ ions have ionic size and weight comparable to those of $Li^+$ ions.

Magnesium metal possesses a number of characteristics which make it attractive as a negative electrode material for rechargeable batteries including highly negative standard potential (−2.375 V versus SHE), relatively low equivalent weight (12 g per Faraday), high melting point (649 °C), low cost, relative abundance, high safety, ease of handling, and low toxicity which allows for urban waste disposal [27]. In resemblance to the rechargeable lithium battery system, the solid-state rechargeable magnesium battery requires $Mg^{2+}$ ion conducting polymer electrolyte. Magnesium sulfate heptahydrate is an inorganic salt with a combination of Mg, S and O and it is also called Epsom salt. Magnesium sulfate is highly soluble in water and solubility is inhibited with lipids typically used in lotions. The anhydrous form is strongly hygroscopic and it can be used as a desiccant. Development and characterization of nano-crystalline composite polymer electrolytes as an alternative to existing electrolytes with improved physical, electrical and testing on lab scale. Development of cost effective sol-gel/electro-spinning technique for membrane fabrication is highly relevant in view of the rapidly increasing conventional alternative sources of energy. To improve the mechanical integrity, solid-state polymer battery has been fabricated with the improved ionic conductivity. In the present work, new polymer electrolyte films have been prepared with PVP complexed with $MgSO_4 \cdot 7H_2O$ and an electrochemical cell has been fabricated with the configuration of anode/polymer electrolyte/cathode and discharge characteristics of the cell were studied for a constant load of 100 kΩ.

## Experimental

### Materials and methods

PVP of average Molecular weight (M.W: 36,000) was purchased from Sigma-Aldrich Chemicals, India. Magnesium sulfate heptahydrate ($MgSO_4 \cdot 7H_2O$) 98% pure was purchased from CDH, India. The salt was dried at 50 °C under vacuum for 48 h and double sterilized water is used as common solvent. The polymer electrolytes were prepared under the following consideration. The weighted amount of PVP (1000 mg) was dissolved in 20 ml of double distilled water under continuous magnetic stirring (30 min) for complete dissolution. The appropriate quantity of $MgSO_4 \cdot 7H_2O$ salts was then added in PVP polymer solution with different compositions of PVP: $x$ wt% $MgSO_4 \cdot 7H_2O$ (where $x$ = 5, 10, 15, 20) and stirred continuously for 24 h. The composite polymer solution was poured in polypropylene Petri dishes and evaporated slowly at room temperature under vacuum drying process to remove the moisture. The obtained thin films were placed in a desiccator until further characterization.

### Characterization

X-ray diffraction (XRD) pattern of the prepared sample was recorded on Bruker D8 instrument with CuKα radiation. Differential scanning calorimetry (DSC) analysis was performed by TA instrument model 2920 "Q". Scanning electron microscopy (SEM) was performed by FE-SEM, Carl Zeiss, Ultra 55 model. Complex impedance spectroscopy measurements were carried out by HIOKI 3532-50 LCR Heister to determine the ionic conductivity and dielectric constant of the polymer electrolyte. Electrochemical cell has been fabricated and its discharge characteristics were studied by Keithley electrometer (Keithley Inc., model 6514) for a constant load of 100 kΩ. The cell parameters were calculated.

## Results and discussion

### XRD studies

X-ray diffraction pattern of the pure PVP and PVP complexed with magnesium sulfate heptahydrate salt is shown in Fig. 1. From the figure, the pure PVP shows a characteristic peak at 21° indicating its semi-crystalline nature. It is observed from the spectrum that the intensity of the crystalline peak of pure PVP gradually decreases with the increase of $MgSO_4 \cdot 7H_2O$ salt. This decrease of degree of crystallinity of the polymer electrolyte with the increasing salt concentration is attributed to the distortion of the semi-crystalline structure of the electrolyte by $MgSO_4 \cdot 7H_2O$ salt. When $MgSO_4 \cdot 7H_2O$ salt is completely dissolved in the PVP polymer, the intensity of broad peak decreases and widens; this implies that the PVP matrix augmented the amorphous domains. As the wt% of $MgSO_4 \cdot 7H_2O$ increases,
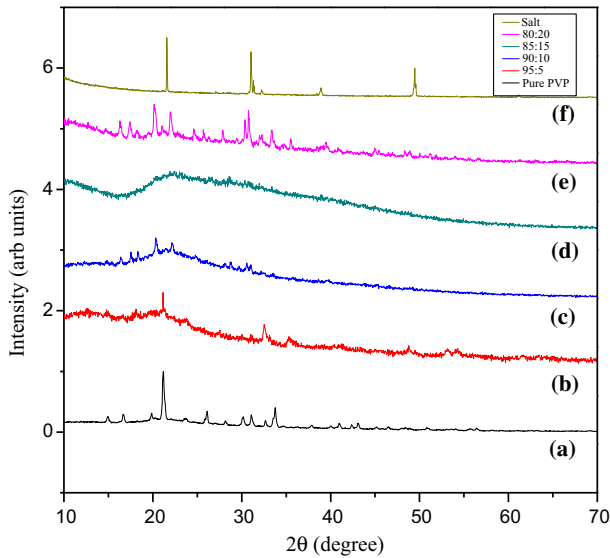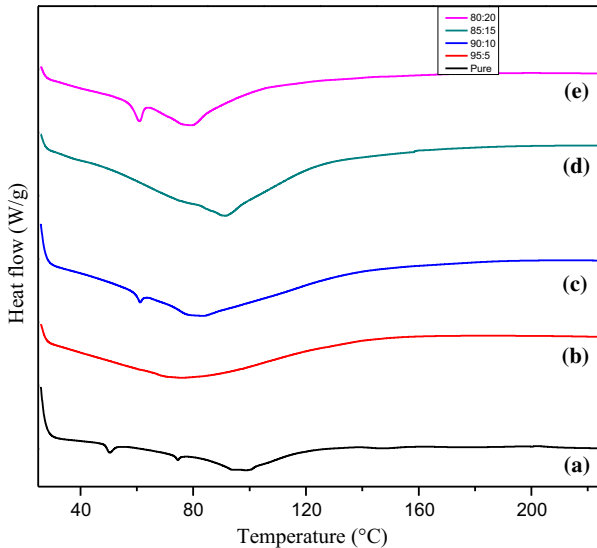
**Fig. 1** XRD analysis of polymer electrolyte films for different wt% ratios of *a* Pure PVP, *b* (95:5), *c* (90:10), *d* (85:15), *e* (80:20), *f* salt

the intensity of the PVP diffraction peak weakens, suggesting that the interaction between PVP chains and salt particles leads to decrease in intermolecular interaction of PVP chains, thereby resulting in increase of the amorphous nature of PVP. The chains are irregular and entangled in amorphous regions, whereas the chains are regularly arranged in crystalline regions. As a result, it is easy to move the molecular chains in the amorphous state compared to the crystalline state and the molecular packing in the amorphous state is weak. Hence, the chains in the amorphous phase are more flexible, orienting themselves relatively more easily and rapidly. This facilitates significant motion of polymer chains in the amorphous phase and complete disappearance of sharp peaks with less intensity, which can be attributed to the amorphous nature of the film. However, when more than 15 wt% of $MgSO_4 \cdot 7H_2O$ salt added into the polymer matrix, new sharp peaks have been appeared, which leads to increase in the viscosity of the polymer electrolyte films. Consequently, the mobility of charge carriers has decreased because of free space for ion transportation is reduced. Hence, the conductivity is decreased.

This is in parallel with the observation of Hodge et al. [28] who investigated the relation between the intensity of the peak and the degree of crystallinity. This increase of amorphous nature with the increase in wt% of salt facilitates $Mg^{2+}$ ions movement in the polymer network. The absence of the peak is related to $MgSO_4 \cdot 7H_2O$ salt concentration in the electrolyte system clearly indicating the complete dissolution of the slat in the polymer matrix. The obtained results are in good agreement with conductivity studies in this work.

## DSC studies

The differential scanning calorimetry curves of pure PVP and PVP complexed with $MgSO_4 \cdot 7H_2O$ for different ratios are shown in Fig. 2. From the figure, it is observed that the melting point for pure PVP is found at 99 °C. It indicates the amorphous nature of the film. By doping the salt concentration to the polymer, the melting temperature $(T_m)$ is decreased predominantly. From the DSC curves, the optimum conduction for low melting point can be determined. The glass transition temperature for different compositions is found to decrease from 99 to 80 °C. The polymer electrolyte films show one endothermic peak at the glass transition temperature. These films exhibit only single $T_g$ values and, hence, it may be concluded that the polymer and salt are miscible completely. By the addition of salt to the PVP, the glass transition temperature is reduced. Due to lubricating effect of the polymer chains the decrease of $T_g$ takes place at lower value. Usually, the amorphous nature of the polymer and its flexibility depends on the glass transition temperature. It is a general notion that the higher flexibility of the polymeric chains or segments is proportional to the lower value of $T_g$. The decrease in $T_g$ helps to soften the polymer backbone and increase its ions through the material when there is an applied electric field [29, 30]. By adding salt to the polymer films, dipole interaction takes place between salt and the polymer chains. As a result, at the melting point the semi-crystalline nature of the salt and the polymer converts into amorphous such that the conductivity nature in polymer film increases.
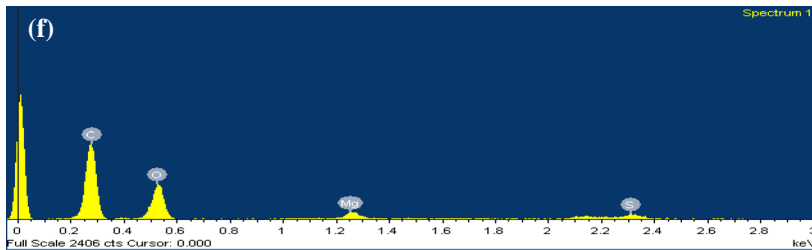


**Fig. 2** DSC spectra of polymer electrolyte films for different wt% ratios of *a* Pure PVP, *b* (95:5), *c* (90:10), *d* (85:15), *e* (80:20)

## SEM analysis

The surface morphology of pure PVP and PVP complexed with $MgSO_4 \cdot 7H_2O$ polymer electrolyte systems was examined using scanning electron microscopy technique. The SEM images of pure PVP and PVP + $MgSO_4 \cdot 7H_2O$ with different wt% ratios (95:5, 90:10, 85:15 and 80:20) have been shown in Fig. 3. The SEM image clearly shows the chunks that are formed in Fig. 3a–e. The $MgSO_4 \cdot 7H_2O$ salt is in completely dissolved in PVP polymer matrix such that no distribution takes place and small chunks are formed. These chunks possess crystalline structure
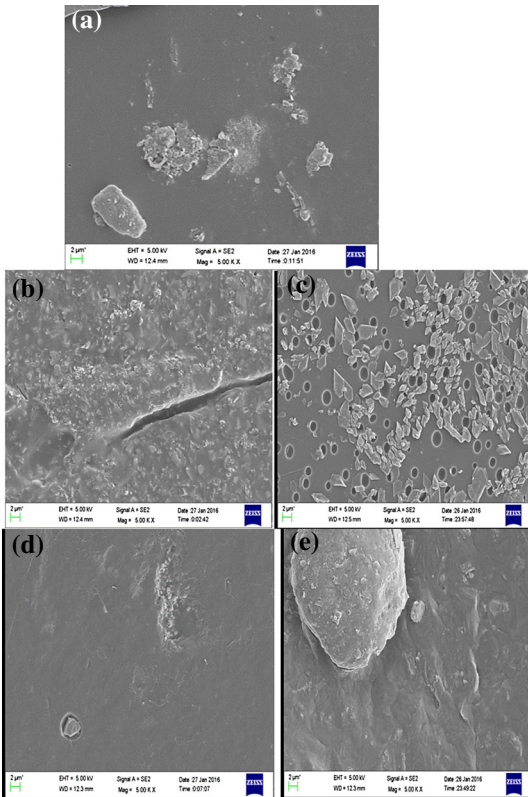


| Element | Weight % | Atomic % |
|---------|----------|----------|
| C | 53.26 | 45.24 |
| O | 27.19 | 42.21 |
| Mg | 12.23 | 9.56 |
| S | 7.09 | 2.02 |
| N | 0.23 | 0.97 |
| Total | 100.00 | 100.00 |

**Fig. 3** SEM images of polymer electrolyte films for different wt% ratios of **a** pure PVP, **b** (95:5), **c** (90:10), **d** (85:15), **e** (80:20), **f** EDS spectra of (85:15) wt% ratio SPE

embedded in the polymer matrix. The presence of crystalline phase in the samples has been observed in XRD pattern as sharp peaks which are attributed to $MgSO_4 \cdot 7H_2O$ salt. But as shown in Fig. 3d, there was no phase separation between PVP polymer and $MgSO_4 \cdot 7H_2O$ salt. This was due to the completely dissolved salt in PVP + $MgSO_4 \cdot 7H_2O$ (85:15) electrolyte system. The smooth surface back ground corresponds to the amorphous nature of the host polymer. The compatibility of the PVP matrix with salt is uniform and homogenous when the salt content is less than 15 wt%. When the salt content is more than 15 wt%, the composites showed a dispersion problem with little agglomeration of particles. This analysis satisfies with the XRD and conductivity studies. The element which is incorporated with the polymer films was analyzed with Energy dispersive spectroscopy (EDS) which is shown in Fig. 3f. The analysis shows the presence of carbon (C), nitrogen (N), sulfur (S), magnesium (Mg) and oxygen (O) elements in the solid polymer electrolyte of PVP + $MgSO_4 \cdot 7H_2O$ (85:15).

## Optical properties

Optical analysis is used to identify the vibrational bands and the transitions of electrons in energy levels. Solid polymer electrolyte thin film has been prepared with the complexation of inorganic salt ($MgSO_4 \cdot 7H_2O$) and the polymer PVP. Absorption coefficient ($\alpha$) was calculated by the following equation

$$I = I_o \exp{(-\alpha x)}. \tag{1}$$

Hence

$$\ln{(I/I_o)} = \alpha x, \quad \alpha = 2.303(A/x), \tag{2}$$

where '$I$' is the transmitted intensity, '$I_o$' is the incident intensity, '$A$' is the absorbance and '$x$' is the thickness of thin film.

To calculate band gap energy values, graphs were plotted between ($\alpha$), $(\alpha h\upsilon)^2$, $(\alpha h\upsilon)^{1/2}$ as a function of ($h\upsilon$). Position of the absorption edge was determined by extrapolating the linear portion of ($\alpha$) versus ($h\upsilon$) curves to zero absorption value. Absorption values for pure PVP, 5, 10, 15 and 20 wt% of $MgSO_4 \cdot 7H_2O$ doped PVP films lie at 4.93, 4.76, 4.49, 4.54 and 4.36 eV, which is observed from Fig. 4a. In case of direct band transitions, the absorption coefficient and energy of incident photon are given by

$$\alpha h\upsilon = C \left(h\upsilon - E_g\right)^{1/2}, \tag{3}$$

where $E_g$ is the energy band gap, $C = 4\pi \, \sigma_o/nc\Delta E$ is a constant which is dependent on the structure of the sample, $\alpha$ is the absorption coefficient, $\upsilon$ is the frequency of incident light and $h$ is a Planck's constant. From the graph $(\alpha h\upsilon)^2$ versus $h\upsilon$ direct band gap values are obtained. Optical band gap values for pure PVP, doped polymer films were 5.2, 5.02, 4.72, 4.81 and 4.65 eV, respectively, as shown in Fig. 4b. In case of indirect transitions, phonon assistance is required for transitions where the absorption coefficient has the following dependence on photon energy [31, 32] which is given by
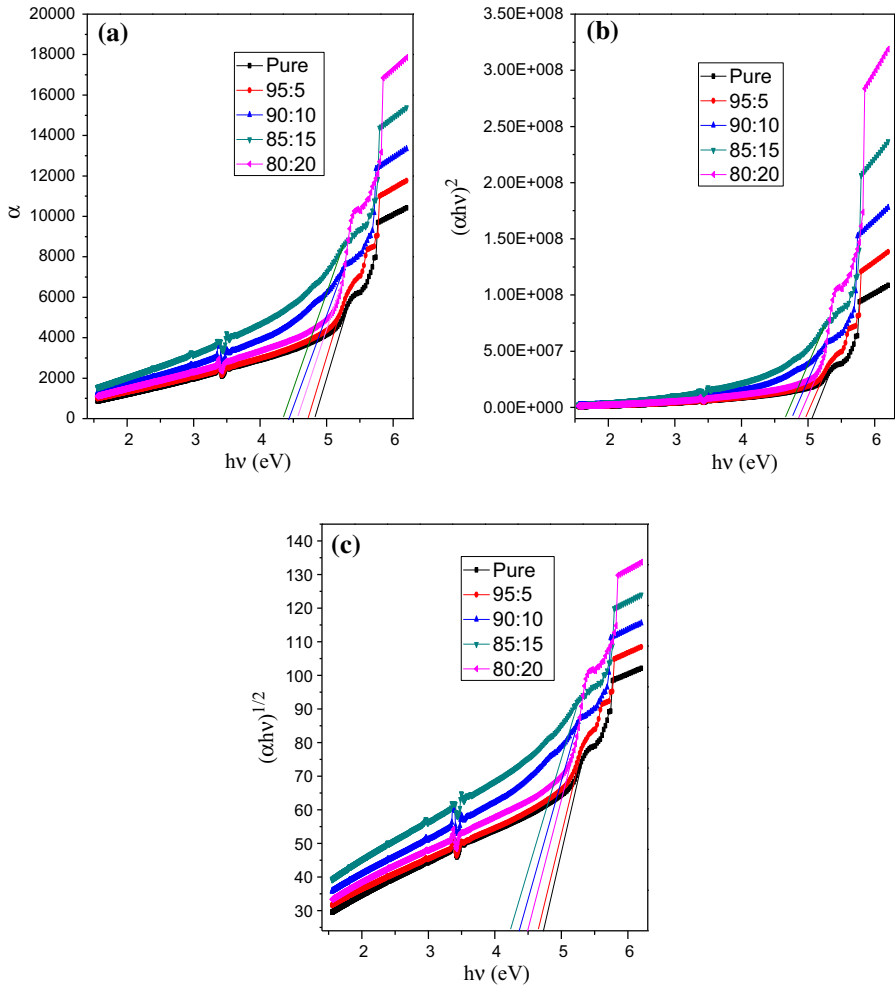
**Fig. 4** **a** α vs *hυ* plots of polymer electrolyte films for different wt% ratios of (a) Pure PVP, (b) (95:5), (c) (90:10), (d) (85:15), (e) (80:20). **b** α vs $(\alpha h\upsilon)^2$ plots of polymer electrolyte films for different wt% ratios of (a) pure PVP, (b) (95:5), (c) (90:10), (d) (85:15), (e) (80:20). **c** α vs $(\alpha h\upsilon)^{1/2}$ plots of polymer electrolyte films for different wt% ratios of (a) pure PVP, (b) (95:5), (c) (90:10), (d) (85:15), (e) (80:20)

$$\alpha h\upsilon = A \left(h\upsilon - E_g - E_p\right)^2 + B \left(h\upsilon - E_g - E_p\right)^2 \tag{4}$$

where $E_p$ is the energy of the photon associated with the transitions, *A* and *B* are constants depending on the band structure. Indirect band gap values were obtained by plotting $(\alpha h\upsilon)^{1/2}$ versus *hυ* as shown in Fig. 4c. Indirect band gap values of pure PVP, doped polymer films obtained from the graph are 5.1, 4.75, 4.43, 4.50 and 4.39, respectively [33]. From the obtained values, it is clear that the dissolution of salt is completely attained in polymer chains in a host lattice; thus, the activation energy is decreased such that the ionic conductivity is increased. The direct and indirect band gap values shifted to lower energies on doping with $MgSO_4 \cdot 7H_2O$ salt

**Table 1** Optical band gap values of MgSO₄·7H₂O solid polymer electrolytes

| Polymer electrolyte | Optical band gap | | Absorption edge |
|---|---|---|---|
| | Direct (eV) | Indirect (eV) | |
| Pure PVP | 5.2 | 5.1 | 4.93 |
| PVP + MgSO₄·7H₂O (95:5) | 5.02 | 4.75 | 4.76 |
| PVP + MgSO₄·7H₂O (90:10) | 4.72 | 4.43 | 4.49 |
| PVP + MgSO₄·7H₂O (85:15) | 4.81 | 4.50 | 4.54 |
| PVP + MgSO₄·7H₂O (80:20) | 4.65 | 4.39 | 4.36 |

to the polymer. The direct, indirect band gap and absorption edge values are presented in Table 1.
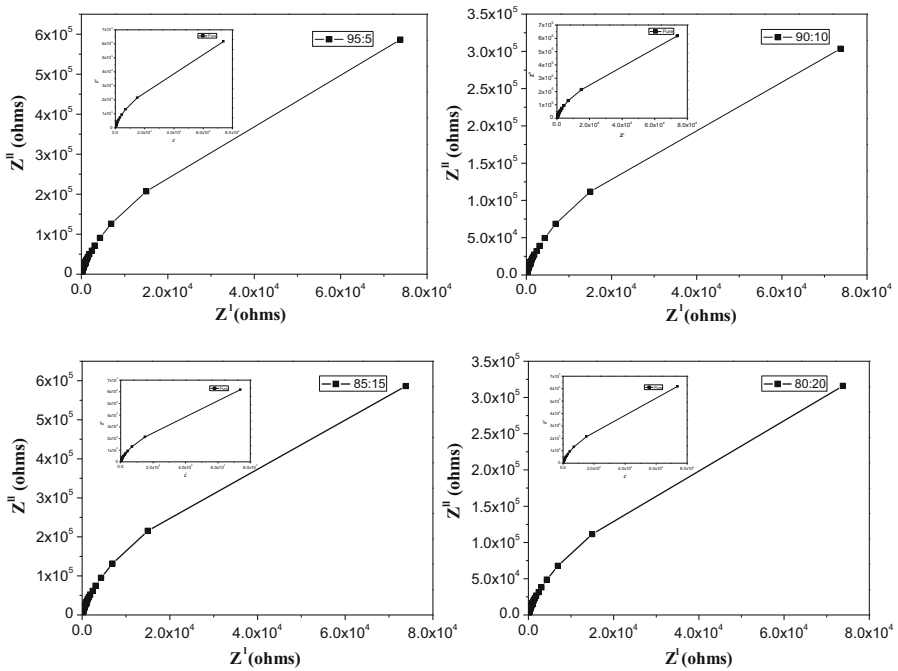
## A.C. conductivity studies

The Cole–Cole plots of the PVP: MgSO₄·7H₂O polymer electrolyte films for different wt% ratios at room temperature (303 K) are shown in Fig. 5. The analysis of Cole–Cole plots has been carried out for the polymer electrolytes using impedance spectroscopy. A small amount of A.C. current is applied across the sample; the variation of imaginary ($Z^{II}$) and real part ($Z^{I}$) can be measured using LCR: HIOKI 3532-50 LCR Heister range from 4 kHz to 5 MHz. The Nyquist plot (Cole–Cole) generally consists of semicircular arc at higher frequency and a spike is formed at lower frequency for the bulk resistance. In the obtained plots, the spike formation can be seen and it is mainly due to ionic conduction [34]. The obtained conductivity values are shown in Table 2. The A.C. conductivity can be calculated from the bulk resistance ($R_b$) which is interrelated by the equation

$$\sigma = t/R_b A, \tag{5}$$

where "$t$" is the thickness of the film, "$A$" is the area of the film and "$R_b$" is the bulk resistance.

The activation energy can be calculated from the conductivity plot which is obtained by the migration of ions. The activation energy plot is shown in Fig. 6. While increasing the temperature, the semi-crystalline nature in the polymer converts the amorphous nature where the transfer of $Mg^{2+}$ ions takes place in the polymer matrix. This amorphous phase produces free volume [35]. The calculated activation energies ($E_a$) of pure PVP and for different compositions of [PVP + MgSO₄·7H₂O] are summarized in Table 3. When compared to other samples, the polymer film PVP + MgSO₄·7H₂O (85:15) has the highest conductivity and lowest activation energy.

**Fig. 5** Cole–Cole plots of polymer electrolyte films for different wt% ratios of **a** pure PVP, **b** (95:5), **c** (90:10), **d** (85:15), **e** (80:20)

**Table 2** AC conductivity values of PVP + MgSO$_4$·7H$_2$O solid polymer electrolytes

| Films | Conductivity at room temperature |
|---|---|
| Pure PVP | $2.32 \times 10^{-9}$ (S/cm) |
| PVP + MgSO$_4$·7H$_2$O (95:5) | $3.15 \times 10^{-7}$ (S/cm) |
| PVP + MgSO$_4$·7H$_2$O (90:10) | $5.12 \times 10^{-7}$ (S/cm) |
| PVP + MgSO$_4$·7H$_2$O (85:15) | $1.05 \times 10^{-5}$ (S/cm) |
| PVP + MgSO$_4$·7H$_2$O (80:20) | $3.42 \times 10^{-6}$ (S/cm) |

## Dielectric properties

The dielectric spectroscopy and impedance analysis studies were carried out using HIOKI 3532-50 LCR Heister in the frequency range from 4 kHz to 5 MHz at room temperature. The conductivity of the sample and the obtained data was analyzed. Figure 7a shows the variation of relative permittivity ($\varepsilon'$) along with the frequency and also concludes by increasing the frequency the relative permittivity ($\varepsilon'$) decreases sharply. Decrease in the dielectric constant with increase in frequency takes place due to polarization at the electrode–electrolyte interfaces. The variation of tangent loss ($\delta$) with log frequency ($f$) for various wt% compositions of the polymer electrolyte samples is shown in Fig. 7b. The decrease in the tangent loss along with increasing the log frequency is obtained; this may be due to the reduced
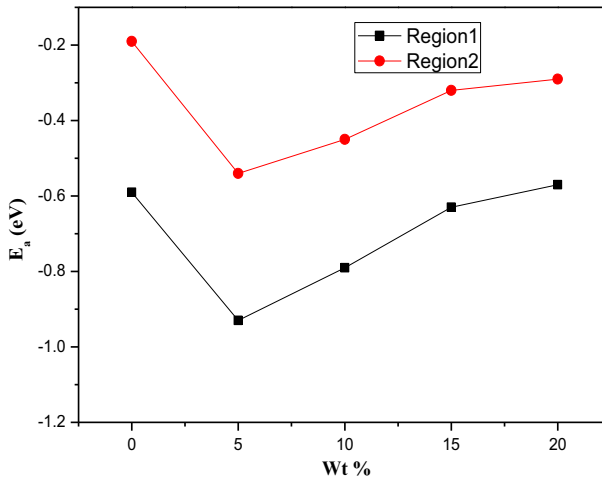
**Fig. 6** Variation of activation energy with MgSO$_4$·7H$_2$O salt concentration wt% ratios at 303 K

**Table 3** Activation energies of PVP + MgSO$_4$·7H$_2$O solid polymer electrolytes

| Films | Region 1 | Region 2 |
|---|---|---|
| Pure PVP | 0.19 | 0.59 |
| PVP + MgSO$_4$·7H$_2$O (95:5) | 0.54 | 0.93 |
| PVP + MgSO$_4$·7H$_2$O (90:10) | 0.45 | 0.79 |
| PVP + MgSO$_4$·7H$_2$O (85:15) | 0.29 | 0.57 |
| PVP + MgSO$_4$·7H$_2$O (80:20) | 0.32 | 0.63 |

proportion of amorphous material leading to reduction in the magnitude of dispersion. The appearance of peaks suggests the presence of relaxing dipoles in the samples and also with electrical relaxation process or inability of dipoles [36].

Figure 7c denotes the fact that when the frequency is increased, the ionic conductivity and the oriental source of polarizability increase due to the transfer of mobile ions causing a constant value of dielectric constant. This may due to large-scale heterogeneity of salt particles which are doped in the complex and replacement by small-scale heterogeneity of salt particles of Mg$^{2+}$; the salt particles are incorporated in the polymer chain complex and it increases the free volume and segmental motion of the polymer chain [37–39]. When the salt particles content is enhanced in the different wt% proportions at higher ratio, segregations of ion take place and it reduces the polarizability of polymer electrolyte system. The change in imaginary part in dielectric permittivity with frequency and Mg$^+$ content is shown in Fig. 7d. The value of $\varepsilon''$ is seen to decrease with increasing frequency at room temperature in nanocomposite polymer electrolyte. Higher the value of imaginary part with respect to frequency, free charge motion takes place at electrode–electrolyte interface [40].

Figure 8 shows the variation of angular frequency with respect to ionic conductivity. It explains the conductivity dependence on the relaxation process and
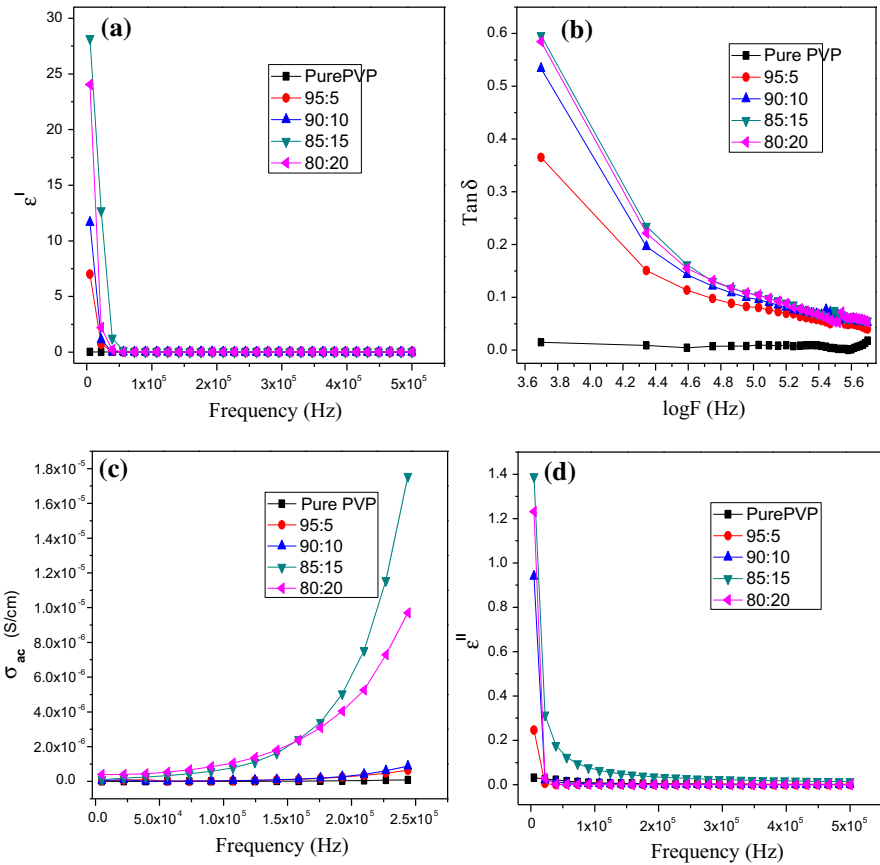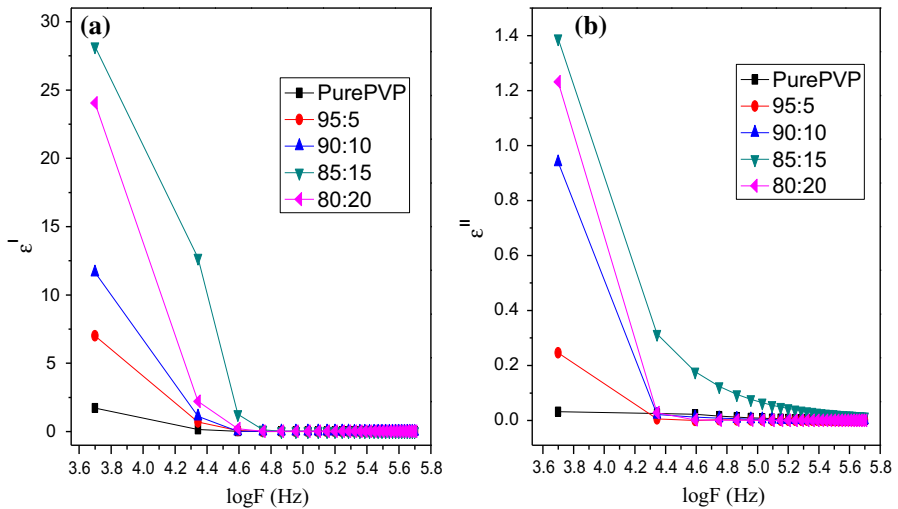
**Fig. 7** **a** Variation of dielectric real part with frequency for different wt% ratios at 303 K. **b** Variation of tangent loss with frequency for different wt% ratios at 303 K. **c** Variation of ac conductivity with the frequency for different wt% ratios at 303 K. **d** Variation of dielectric loss imaginary part with the frequency for different wt% ratios at 303 K

it is non-exponential in time. The plateau region describes the space charge polarization at the blocking electrode and is associated with ac conductivity ($\sigma_{ac}$) of the complexed polymer electrolyte. As shown in Fig. 8, the high frequency dispersion region, the ionic conductivity increases with the increase in frequency which is associated with conductivity $\sigma_{ac}$ of the polymer electrolyte. However, at high frequencies the conductivity variation with temperatures is much less than that of lower frequencies [41, 42]. Figure 9a, b shows the variation of frequency with dielectric constant. The dielectric constant decreases gradually with increasing frequency and found to be high for the sample 15 wt% due to drifting of ions which results in high conductivity. This reveals that the salt is completely dissolute in the polymer chains giving raise to mobile ions. Due to the formation of space charge region at the electrode–electrolyte interface a variation is observed in between
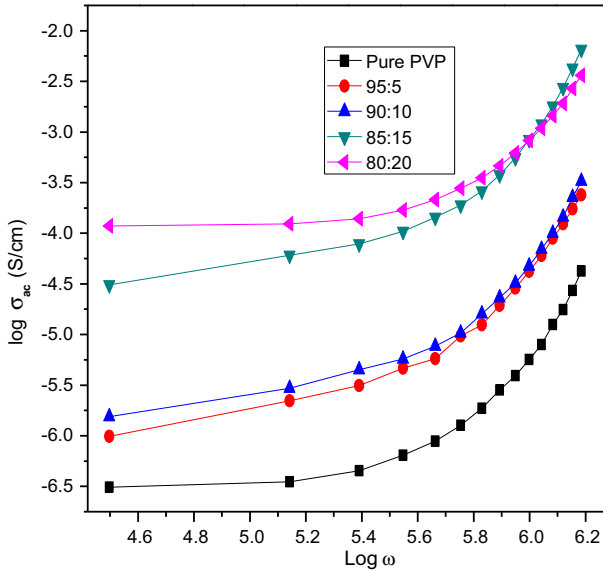
**Fig. 8** Variation of log ac conductivity with log frequency for different wt% ratios at 303 K



**Fig. 9 a, b** Variation of log F with dielectric permittivity for different wt% ratios at 303 K

dielectric constant $\varepsilon'$ and the frequency which is dependent on both electrolytes and is proportional to $\omega n^{-1}$, indicating non-Debye behavior [43–47].

Figure 10 shows the variation of tangent loss with frequency of polymer films for different wt% ratios of PVP at room temperature. The loss spectra characterized by peak appearing at a characteristic frequency for polymer samples suggest the relaxation dipole; the strength and frequency of the relaxation depend on the

**Fig. 10** Variation of tangent loss with frequency for different wt% ratios at 303 K
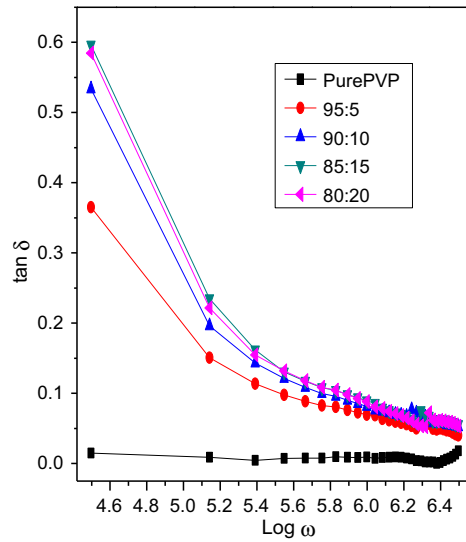
characteristic property of dipole relaxation. The tangent loss peaks shift towards the higher frequency [48]. It is evident that the peak is shifted towards higher frequency side, thereby reducing the relaxation time.

The dielectric constant of different wt% ratios of samples as a function of room temperature is shown in Fig. 11a–c. The dielectric constant of composite electrolytes increases apparently with the increase of temperature. The increment of dielectric constant peaks is observed at room temperature. The abrupt change in dielectric constant has been verified by the conductivity. This is due to the ionic jump orientation, space charge polarization and electronic contribution of $Mg^{2+}$ ions. [49]. Figure 12a, b shows the variation of dielectric permittivity with the frequency of the PVP: $MgSO_4 \cdot 7H_2O$ polymer electrolyte at room temperature. From the figures, it is observed that with the increase in frequency the dielectric permittivity decreases monotonically. At higher frequencies, the dielectric values remain constant and the similar behavior is observed in reaming samples, which could be due to the dipole interaction and electrode–electrolyte polarization effects. At higher frequencies, the ionic diffusion does not take place in the direction of the field.

**Transport properties**

To evaluate the nature of species responsible for conductivity in the present electrolyte system, the transport numbers (which give a quantitative assessment of the extent of the ionic and electronic contributions to the total conductivity) were measured by applying a constant d.c. potential of 1.5 V across the cell. Figure 13 shows the polarization current versus time plot. As seen from the plot, the current ($i_t$) rises at the very beginning of polarization, then decays immediately and asymptotically approaches steady state after a long time. The transference number
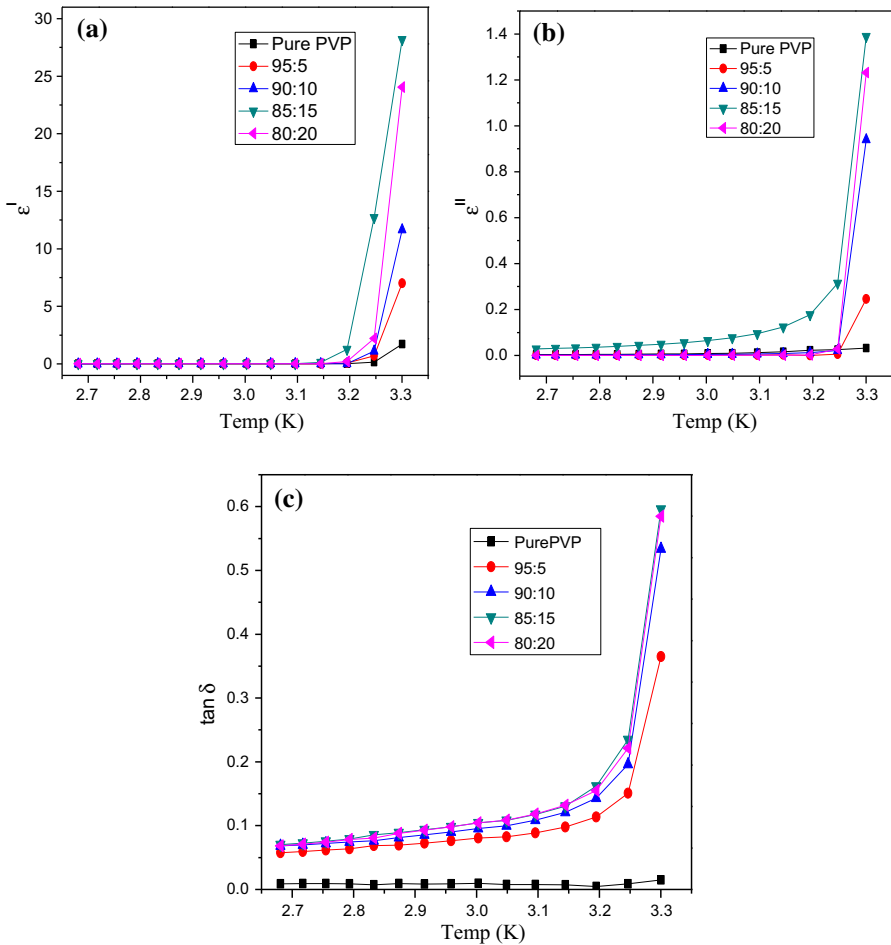
**Fig. 11** **a**, **b** Variation of temperature with dielectric permittivity for different wt% ratios at 303 K. **c** Variation of temperature with tanδ for different wt% ratios at 303 K

corresponding to $t_{ion}$ and $t_{ele}$ transport has been calculated by Wagner's polarizing technique. The transference number ($t_{ion}$ and $t_{ele}$) is calculated from the polarization current verses time plot using the equation

$$t_{ion} = i_t - i_{ele}/i_t \quad \text{and} \quad t_{ele} = i_{ele}/i_t, \tag{6}$$

where $i_t$ is the initial current and $i_{ele}$ is the final residual current of solid polymer electrolyte. The transference number $t_{ion}$ is found to be 0.98 for 85:15 wt% ratios. It results that the charge transport taking place in these polymer films is mainly due to ions, as well as residual of electrons also takes place.
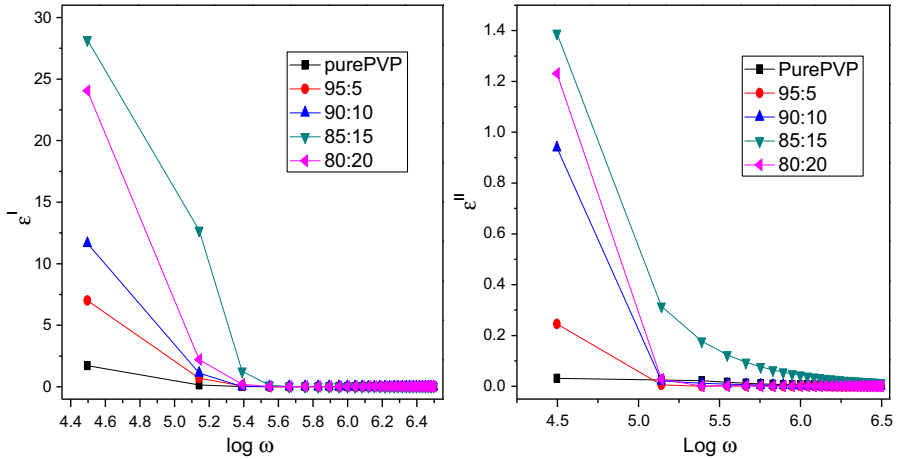
**Fig. 12** **a**, **b** Variation of dielectric permittivity with the frequency for different wt% ratios at 303 K
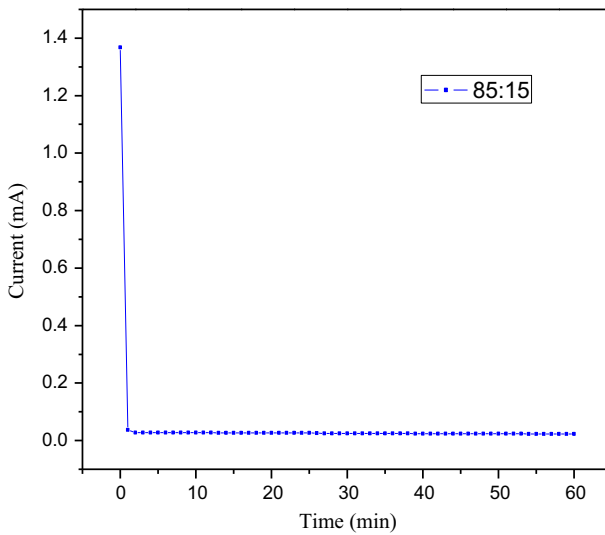


**Fig. 13** Transport properties of polymer electrolyte film for 85:15

## Discharge characteristics

Solid-state polymer battery has been fabricated for a constant load of 100 kΩ with the configuration of $Mg^+$ (anode)/[PVP + $MgSO_4 \cdot 7H_2O$]electrolyte/ ($I_2$ + C + electrolyte) for different compositions (95:5), (90:10), (85:15) and (80:20) as shown in Fig. 14. In the polymer battery, magnesium metal was used as anode and theproper mixture of iodine, graphite and electrolyte traces in the ratio (5:5:1) is used as cathode which enhances its electronic conductivity. Current density was calculated
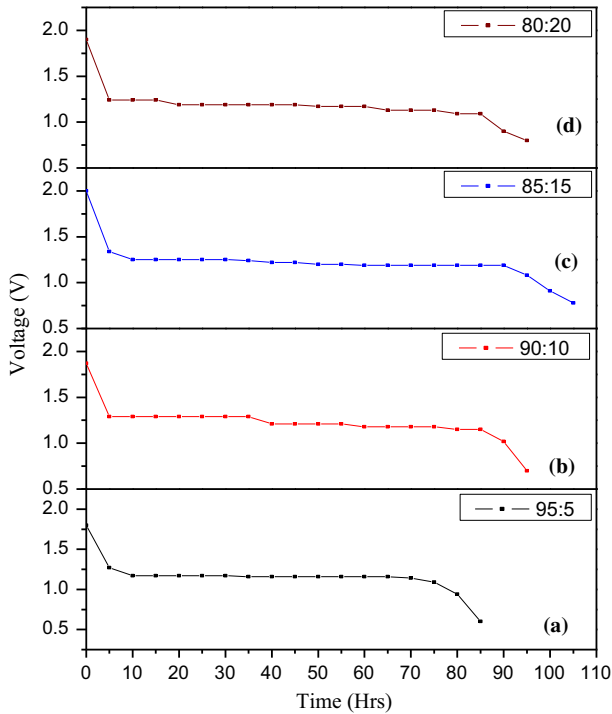
**Fig. 14** Discharge characteristics of polymer electrolyte films for different wt% ratios of *a* pure, PVP, *b* (95:5), *c* (90:10), *d* (85:15), *e* (80:20)

using short circuit value and the area of the cell. Power density values were obtained by taking weight of the cell into consideration. Energy density values were calculated by evaluating the time taken for plateau region. Initially, a rapid decrease in the voltage is occurred; it may be due to the polarization and the formation of thin layer of magnesium salt at the electrode–electrolyte interfaces [50]. From the data, it is clear that the open-circuit voltage was found to be greater in PVP + MgSO$_4$·7H$_2$O (85:15) cell compared to other complexed films. This may be due to the high ionic conductivity the system when compared to other systems. While increasing wt% of the salt concentration, the open-circuit voltage and discharge time of the cell for the polymer electrolyte increase predominantly. From the conductivity studies, it is clear that the salt concentration of 15 wt% has the large discharge time. For all the electrochemical cells based on [PVP + MgSO$_4$·7H$_2$O] electrolyte, open-circuit voltage (OCV), short circuit current (SCC) and the other cell parameters have been evaluated form the discharge characteristic curves and the data are tabulated in Table 4.

**Table 4** Cell parameter values of PVP + MgSO$_4$·7H$_2$O of solid polymer electrolyte system

| Parameters | 95:05 | 90:10 | 85:15 | 80:20 |
|---|---|---|---|---|
| Cell weight (g) | 1.31 | 1.31 | 1.31 | 1.31 |
| Area of the cell (cm$^2$) | 1.42 | 1.42 | 1.42 | 1.42 |
| Open-circuit voltage (OCV) | 1.80 | 1.87 | 2.00 | 1.90 |
| Discharge time (h) | 87 | 98 | 108 | 95 |
| Current density (mA/cm$^2$) | 0.84 | 0.83 | 0.82 | 0.81 |
| Discharge cell (mA/h) | 13.7 | 12.2 | 11.1 | 12.6 |
| Power density (W/kg) | 1.64 | 1.58 | 1.69 | 1.60 |
| Energy density (W h/kg) | 142.68 | 154.84 | 182.52 | 152.24 |

## Conclusions

Solid-state polymer electrolyte of Mg$^{2+}$ was prepared by PVP complexed with MgSO$_4$·7H$_2$O salt by solution cast technique. The structural analysis of pure PVP complexed with MgSO$_4$·7H$_2$O salt showed crystalline orthorhombic lattice indicating its semi-crystalline nature. SEM images reveal the heterogeneous phase of nanocomposite polymer electrolyte systems. From the optical analysis, it is revealed that the films with the lower activation energy have the highest ionic conductivity. From the conductivity studies, the highest conductivity for PVP + MgSO$_4$·7H$_2$O (85:15) was found to be $1.05 \times 10^{-5}$ (S/cm) at room temperature. Using these polymer electrolyte films, a solid-state battery has been fabricated and the discharge characteristics were studied.

## References

1. Tsutsumi H, Suzuki A (2014) Cross-linked poly (oxetane) matrix for polymer electrolyte containing lithium ions. Solid State Ion 262:761–764
2. Wu HY, Chen YH, Saikia D (2013) Synthesis, structure and electrochemical characterization and dynamic properties of double core branched organic–inorganic hybrid electrolytes membranes. J Membr Sci 447:274–286
3. Nazeeruddin MK, Kay A, Rodicio I, Humphry-Baker R, Mueller E, Liska P, Vlachopoulos N, Gratzel M (1993) Conversion of light to electricity by cis-X$_2$bis(2,2′-bipyridyl-4,4′-dicarboxylate)ruthenium(II) charge-transfer sensitizers (X = Cl-, Br-, I-, CN-and SCN-) on nanocrystalline titanium dioxide electrodes. J Am Chem Soc 115:6382–6390
4. Bhattacharya B, Lee JY, Geng J, Jung HT, Park JK (2009) Effect of cation size on solid polymer electrolyte based dye-sensitized solar cells. Langmuir 25:3276–3281
5. Zheng T, Zhou Q, Li Q (2014) A new branched copolyether-based polymer electrolyte for lithium batteries. Solid State Ion 259:9–13
6. Nagarale RK, Bhattacharya B, Jadhav NA, Singh PK (2011) Synthesis and electrochemical study of a functional ionic polymer. Macromol Chem Phys 212:1751–1759
7. Croce F, Appetecchi GB, Persi L, Scrosati B (1998) Nanocomposite polymer electrolytes for lithium batteries. Nature 394:456–462
8. Macdonald JR, Potter D (1987) A flexible procedure for analyzing impedance spectroscopy results: description and illustrations. Solid State Ion 23:61–79
9. Kalaignan GP, Kang MS, Kang YS (2006) Effects of compositions on properties of PEO–KI–I$_2$ salts polymer electrolytes for DSSC. Solid State Ion 177:1091–1097

10. Zhou X, Yin Y, Wang Z (2011) Effect of hot pressing on the ionic conductivity of the PEO/LiCF$_3$SO$_3$ based electrolyte membranes. Solid State Ion 196:18–24

11. Keddie JL, Jones RAL, Cory RA (1994) Size-dependent depression of the glass transition temperature in polymer films. Euro Phys Lett 27:59–64

12. Ellison CJ, Torkelson JM (2003) The distribution of glass-transition temperatures in nanoscopically confined glass formers. Nat Mater 2:695–700

13. Ted M, Pappenfus Wesley A, Henderson Owens BB (2004) Ionic conductivity of a poly (vinylpyridinium)/silver iodide solid polymer electrolyte system. Solid State Ion 171:41–44

14. Mann Kent R, William H, Smyrl S, Rao Sreepathi, Subba Rao UV (1994) Preparation and characterization of a new polymer battery using PA+ AgNO$_3$ electrolyte. J Mater Sci Lett 13:1771–1772

15. Abdelrazek EM (2004) Physical properties of MgCl$_2$-filled PMMA films for optical applications. Phys B 351:83–89

16. Pandey GP, Agrawal RC, Hashmi SA (2011) Ionic liquid mediated magnesium ion conduction in poly (ethylene oxide) based polymer electrolyte. Electrochim Acta 56:3864–3873

17. Chu D, Jiang RJ (1999) Comparative studies of polymer electrolyte membrane fuel cell stack and single cell. J Power Sources 80:226–234

18. Singh Manjeet, Singh Vivek K, Surana Karan, Bhattacharya B, Singh Pramod K, Rhee HW (2013) New polymer electrolyte for electrochemical application. J Ind Eng Chem 19:819–822

19. Tomar Ritu, Sharma Chirag R (2014) Studies on conducting PVP polymer composites for AC conduction. Int J Sci Eng Technol Res 3:3023–3026

20. Mohamad SA, Yahya R, Ibrahim ZA, Arof AK (2007) Photovoltaic activity in a ZnTe/PEO–chitosan blend electrolyte junction. Ionics 91:1194–1198

21. Agrawal RC, Pandey GP (2008) Experimental investigations on a proton conducting nanocomposite polymer electrolyte. J Phys D Appl Phys 41:055409

22. Hodge RM, Edward GH, Simon GP (1996) Water absorption and states of water in semicrystalline poly (vinyl alcohol) films. Polym 37:1371–1376

23. Morales E, Acosta JL (1997) Thermal and electrical characterization of plasticized polymer electrolytes based on polyethers and polyphosphazene blends. Solid State Ion 96:99–106

24. Cheng Q, Cui Z, Li J (2014) Preparation and performance of polymer electrolyte based on poly (vinylidene fluoride)/polysulfone blend membrane via thermally induced phase separation process for lithium ion battery. J Power Sources 266:401–413

25. Reddeppa N, Sharma AK, Rao VVRN (2014) AC conduction mechanism and battery discharge characteristics of (PVC/PEO) polyblend films complexed with potassium chloride. Measurement 47:33–41

26. Arof AK, Amirudin S, Yusof SZ (2014) A method based on impedance spectroscopy to determine transport properties of polymer electrolytes. Phys Chem Chem Phys 16(5):1856–1867

27. Williamson MJ, Southall JP, Hubbard HVSA (1998) NMR measurements of ionic mobility in model polymer electrolyte solutions. Electrochim Acta 43:1415–1420

28. Ramesh S, Arof AK (2001) Structural, thermal and electrochemical characteristics of poly vinyl chloride (PVC) based polymer electrolytes. J Power Sources 99:41–47

29. Davis PW, Shilliday TS (1960) Some optical properties of cadmium telluride. Phys Rev 118:1020–1022

30. Thutupalli GKM, Tomlin SG (1976) The optical properties of thin films of cadmium and zinc selenides and tellurides. J Phys D Appl Phys 9:1639–1646

31. Sk Shahenoor Basha, Sunita Sundari G, Vijaya Kumar K (2016) Studies on electrical properties of potassium acetate complexed with polyvinyl alcohol for electrochemical cell applications. Mater Today Proc 3:11–20

32. Venkata Subba Rao C, Ravi M, Raja V, Balaji Bhargav P, Sharma Ashok Kumar, Narasimha Rao VVR (2012) Preparation and characterization of PVP-based polymer electrolytes for solid-state battery applications. Iran Polym J 21:531–536

33. Sk Shahenoor Basha, Sunita Sundari G, Vijaya Kumar K (2016) Effect of Al$_2$O$_3$ on PVP based polymer electrolyte films doped with MgCl$_2$·6H$_2$O for solid state battery applications. Int J Chem Tech Res 9:383–391

34. Diilip K, Pradhan RNP, Chowdary B, Samantaray K (2008) Studies of dielectric relaxation and AC, conductivity behavior of plastisized polymer nano composite electrolytes. Int J Electrochem Sci 3:597–608

35. Mohd Z, Iqbal R (2016) Structural.electrical conductivity and dielectric behavior of Na$_2$SO$_4$-LDT Composite solid electrolyte. J Adv Res 7:135–141

36. Kamalesh P (2011) Development of magnisio ferrite doped polymer electrolyte system for battery applications. Int J Mat Sci 1:9–17
37. Deraman SK, Mohamed NS, Subban RHY (2014) Ionic liquid incorporated PVC based polymer electrolytes: electrical and dielectric properties. Sains Malays 43:877–883
38. Anji Reddy P, Ranver Kumar K (2011) AC-Impedence and dielectric spectroscopic studies of $Mg^{2+}$ ion conducting PVA-PEG blended polymer electrolytes. Bull Mater Sci 34:1063–1067
39. Melagiriyappa E, Veena M, Somasekharappa AG, Shankara Murthy J, Jayanna HS (2014) Dielectric behavior and ac electrical conductivity in samarium substituted Mg–Ni ferrites. Ind J Phys 88:795–801
40. Hema M, Selvasekarapandian S, Arun Kumar D, Sankuntala A, Nithya H (2009) FTIR, XRD and AC impedence spectroscopic study on PVA based polymer electrolyte doped with $NH_4X$ (X = Cl, Br, I). J Non Cryst Solids 355:84–90
41. Austin Suthanthiraj S, Joice Sheeba D, Joseph Paul B (2009) Impact of ethylene carbonate onion transport characteristics of $PVdF–AgCF_3SO_3$ polymer electrolyte system. Mater Res Bull 44:1534–1539
42. Bhaskaran R, Selavasekarapandiam S, Kuwata N, Kawamura Hattori JT (2006) AC Impedance, DSC and FT-IR investigations on $(x)PVAc–(1 − x)PVdF$ blends with $LiClO_4$. Mater Chem Phys 98:55–61
43. Ramesh S, Pohling O (2010) Effect of ethylene carbonate on the ionic conduction in poly (vinylidenefluoride-hexafluoropropylene) based solid polymer electrolytes. Polym Chem 1:702–707
44. Rajendran S, Babu Ravi Sankar, Siva Kumar P (2008) Investigations on PVC/PAN composite polymer electrolytes. J Membr Sci 315:67–73
45. Ravinder D, Ramana Reddy AV, Ranga Mohan G (2002) Abnormal dielectric behaviour in polycrystalline zinc substituted manganese ferrites at high frequencies. Mater Lett 52:259–265
46. Yang CC (2006) Study of alkaline nanocomposite polymer electrolytes based on $PVA–ZrO_2–KOH$. Mater Sci Eng B 131:256–262
47. Chandra A, Agrawal RC, Mahipal YK (2009) Ion transport property studies on PEO–PVP blended solid polymer electrolyte membrane. J Phys D Appl Phys 42:135107
48. Shukla N, Awalendra K, Thakur Shukla A, Marx DT (2014) Ion conduction mechanism in solid polymer electrolyte: an applicability of almond-west formalism. Int J Electrochem Sci 9:7644–7659
49. Qian X, Gu N, Zhiliang C (2001) Methods to study the ionic conductivity of polymeric electrolytes using a.c impedance spectroscopy. J Solid State Electrochem 6:8–15
50. Kiran Kumar K, Ravi M, Pavani Y, Bhavani S, Sharma AK, Narasimha Rao VVR (2014) Investigations on PEO/PVP/NaBr complexed polymer blend electrolytes for electrochemical cell applications. J Membr Sci 454:200–211